NMR Dynamics of PSE-4 β-Lactamase: An Interplay of ps-ns Order and μs-ms Motions in the Active Site

Sébastien Morin and Stéphane M. Gagné*
Département de Biochimie et de Microbiologie and PROTEO, Université Laval, Québec, Canada

ABSTRACT The backbone dynamics for the 29.5 kDa class A β-lactamase PSE-4 is presented. This solution NMR study was performed using multiple field ^{15}N spin relaxation and amide exchange data in the EX2 regime. Analysis was carried out with the relax program and includes the Lipari-Szabo model-free approach. Showing similarity to the homologous enzyme TEM-1, PSE-4 is very rigid on the ps-ns timescale, although slower μs-ms motions are present for several residues; this is especially true near the active site. However, significant dynamics differences exist between the two homologs for several important residues. Moreover, our data support the presence of a motion of the Ω loop first detected using molecular dynamics simulations on TEM-1. Thus, class A β-lactamases appear to be a class of highly ordered proteins on the ps-ns timescale despite their efficient catalytic activity and high plasticity toward several different β-lactam antibiotics. Most importantly, catalytically relevant μs-ms motions are present in the active site, suggesting an important role in catalysis.

INTRODUCTION

The main resistance mechanism against penicillin-derived molecules (the β-lactams) is the production of enzymes, the β-lactamases, able to cleave the four-membered β-lactam ring (1). Enzymes from class A are the most often found (2), representing a diverse class of proteins in terms of substrate specificity. Moreover, these 30 kDa enzymes are highly effective catalysts, some with a diffusion-controlled specific activity (3).

Class A β-lactamases general mechanism is composed of two steps akin to that of serine proteinases (4). First, catalytic Ser^{70} makes a nucleophilic attack on the carbonyl of the β-lactam ring. This leads to the hydrolysis of the β-lactam ring after acylation to the protein (1). The process is similar when β-lactam antibiotics inactivate their target, ending up in an inactive acyl-enzyme complex that stops bacterial cell growth and leads to cell death. The second step, a deacylation, which is virtually absent for DD-transpeptidases, consists of a nucleophilic attack by a H_2O molecule activated by the conserved residue Glu^{166}, part of the Ω loop (Arg^{161} to Asp^{179}) (1). This leads to the hydrolysis of the acyl-enzyme complex and release of the hydrolyzed β-lactam.

To attack the β-lactam ring, the catalytic Ser^{70} must have its hydroxyl proton accepted by a general base. The identity of this activator is, however, controversial. One hypothesis involves Lys^{73} as the general base whereas another involves Glu^{166} (1). Other studies proposed the involvement of Ser^{130} (5). A new model has emerged recently in which a duality of mechanisms was shown for tetrahedral formation (6), meaning that the activation process could depend on the β-lactamase/β-lactam combination. A deeper understanding of the structure/function relationship in β-lactamases may help in validating and reinforcing this hypothesis. More specifically, the knowledge of the motions arising in these proteins, especially near the active site, should provide a better mechanistic understanding and complement structural data. Several molecular dynamics (MD) studies have been performed to get insights into the function/structure/dynamics link of class A β-lactamases. These studies have focused on TEM-1.

NMR is a powerful tool for the study of protein dynamics. It allows atom-specific data to be gathered for movements as fast as side-chain rotations or hydrogen-bond formation, and as slow as protein folding. Studying movements of N-H bonds provides a specific probe for almost all residues. ^{15}N spin relaxation rates depend mainly on the N-H bond reorientations with respect to the external magnetic field as a function of time (7), allowing the study of the information-rich ps-ns and μs-ms timescales. It is known that motions arising on the ps-ns timescale influence the thermodynamics of ligand binding, as well as the kinetics of catalyzed reactions (8). Moreover, motions on the μs-ms timescale are directly linked to enzyme catalysis (9).

As of today, only one class A β-lactamase, TEM-1, has had its backbone dynamics characterized by NMR. TEM-1 is the model enzyme for traditional class A β-lactamases. Savard and Gagné (10) demonstrated that TEM-1 is a very rigid protein on the ps-ns timescale. This rigidity is especially important near the active site, presuming that substrate binding should not trigger any important unfavorable loss in conformational entropy. In addition, μs-ms motions were observed around the active site and Ω loop. Further insights into TEM-1 dynamics were obtained by a study on the comparative dynamics of the wild-type enzyme with the mutant $Tyr^{105}Asp$ (11). It was shown that this single point mutation could have long-range effects on the dynamics of the protein.

Submitted July 11, 2008, and accepted for publication February 25, 2009.

*Correspondence: stephane.gagne@bcm.ulaval.ca

Editor: Josh Wand.

© 2009 by the Biophysical Society

0006-3495/09/06/4681/11 $2.00

doi: 10.1016/j.bpj.2009.02.068

Here, we add to these two studies by presenting the backbone dynamics of the carbenicillin hydrolyzing class A β-lactamase PSE-4 as obtained by NMR. PSE-4 enzyme was originally found in *Pseudomonas aeruginosa* (12), an opportunistic pathogen, but was soon found in nonpseudomonal strains (13). It is the model enzyme for the subclass of carbenicillin hydrolyzing class A β-lactamases. The crystal structure of this 271-residue protein (29.5 kDa) was determined previously (14). Besides PSE-4 having a high sequence identity with TEM-1 (41.5%), its structure (composed of two domains: an all α- and an α/β domain) is also very close to that of TEM-1 with a backbone RMSD of 1.3 Å.

We supply data on PSE-4 dynamics from amide exchange as well as ^{15}N spin relaxation data analyzed using the Lipari-Szabo model-free approach (15,16). Additionally, the assessment of data sets consistency, a prerequisite for multiple field data analysis, is discussed in the context of the data presented in this work.

METHODS

NMR data acquisition

^{15}N-labeled PSE-4 was produced as described previously (17). NMR samples were as follows: 0.5 mM PSE-4, 10% D_2O, 3 mM imidazole, and 0.1% sodium azide at pH 6.65. Chemical shift referencing was performed externally using a sample of 0.4 mM 2,2-dimethyl-2-silapentane-5-sulfonic acid (DSS) in 10% D_2O. Spectra were acquired at a temperature of 31.5°C (calibrated using MeOH) on a Varian INOVA 600 (in-house), and Varian INOVA 500 and 800 (Québec/Eastern Canada High Field NMR Facility, Montréal, Canada) spectrometers (corresponding to 60.8, 50.6, and 81.0 MHz nitrogen frequency, respectively) equipped with z axis, pulsed-field gradient, triple-resonance cold probes (except for amide exchange data at pH 7.85, which was acquired using a room temperature probe).

Measurement of longitudinal (R_1) and transversal (R_2) relaxation rates as well as the steady-state heteronuclear nuclear Overhauser effect (NOE) proceeded with established pulse sequences (18,19). Details are available in the Supporting Material. For both R_1 and R_2 experiments, acquisition of relaxation data was made in an interleaved manner to prevent the effects of field and sample inhomogeneity as a function of time (20). NOEs were made in duplicate at 50.6 MHz. At 60.8 MHz, R_1 experiments were made in quadruplicate, R_2, in quintuplicate, and NOE, in triplicate, with some experiments recorded before and others after the recording of data at 50.6 and 81.0 MHz. This ensured that the sample was in the same state throughout the complete experimental scheme.

Amide exchange experiments proceeded from TROSY-HSQC spectra (BioPack, Varian, Palo Alto, CA) of lyophilized PSE-4 dissolved in D_2O. The TROSY implementation allowed smaller phase cycling so very short spectra could be acquired with limited baseline distortions. At the beginning, more frequent short spectra (with a low number of transients) were acquired, and at the end, fewer long spectra (with increasing transients) were acquired. To determine the exchange regime, amide exchange experiments were performed for 80 days at pH 6.65, and for six days at pH 7.85. In both situations, 60 spectra were recorded. Details can be found in the Supporting Material.

NMR data processing

NMR data were processed using the program NMRPipe (21). Details are available in the Supporting Material. Peak deconvolution proceeded using the macro nlinLS invoked from the script autoFit.tcl, both distributed within NMRPipe (21). R_1 and R_2, as well as amide exchange rates, were obtained with the program CURVEFIT (A. G. Palmer, Columbia University, New York, NY). Errors on these fits were obtained from either 500 Monte Carlo simulations or the Jackknife method, using the method that yielded the largest error. A correction was introduced for systematic errors not accounted for when a near-perfect fit was obtained from the R_1 and R_2 exponential curve-fitting. This was done only for model-free analysis where too small errors on experimental data can introduce overcomplex models. Thus, parameters with unrealistically small errors (smaller than the mean value) had their error scaled to the mean value. This is similar to what was done in Savard and Gagné (10). Finally, NOEs were calculated as the ratio of peak amplitude with and without proton saturation, and error propagation calculated from the noise.

Consistency test

Consistency between data sets acquired at different magnetic fields was assessed with the use of reduced spectral density mapping (22) within the program relax (Ver. 1.2.14) (23,24). The test consisted of calculating the field-independent function $J(0)$ for each residue and then comparing results obtained at different fields. For these calculations, the ^{15}N chemical shift anisotropy (CSA) was −172 ppm, and the vibrationally averaged effective N-H bond length (r_{N-H}) was 1.02 Å.

Model-free analysis

Model-free analysis of relaxation data was performed using the program relax (Ver. 1.2.14) (23,24) with a variant of the methodology for the dual optimization of the model-free parameters and the global diffusion tensor proposed recently (24) (see Fig. S4 in the Supporting Material). To avoid any artifact (resulting from under- or overfitting), only residues for which data were available at the three magnetic fields were analyzed. N-H vectors orientations were extracted from PDB 1G68 (14). Values for the CSA and r_{N-H} were the same as for the consistency test. This is as in Savard and Gagné (10), for comparison purposes with dynamics of the homologous protein TEM-1.

Five different diffusion tensors were tested (no global diffusion tensor with a local τ_m parameter for each residue, sphere, prolate spheroid, oblate spheroid, and ellipsoid). These were optimized using residues from well-defined secondary structures (determined using DSSP (25), see Table S3 in the Supporting Material) and selected by Akaike information criterion (AIC) (26). Selection of local model-free models (described in the Supporting Material) during iterations for diffusion tensor optimization was also done using AIC. This allowed the selection of complex models for residues difficult to fit, avoiding the diffusion tensor from being biased by those residues. After convergence of the different diffusion tensors and selection of that with the lowest AIC, local model-free models were minimized for all residues using this diffusion tensor, which was then held fixed. Then, the best model for each residue was selected using the small sample size-corrected (AIC_c) (27). This was done to minimize overfitting which could lead to overinterpretation of relaxation data. Finally, errors on the extracted local parameters were obtained by performing 500 Monte Carlo simulations. A flowchart of the model-free protocol used in this study is available in Fig. S4.

Sequence numbering

Using the Ambler numbering scheme (28), mature PSE-4 starts at residue 22 and ends, after 271 residues and three gaps (positions 58, 239, and 253), at residue 295.

RESULTS AND DISCUSSION

Chemical shift referencing was done externally because DSS interacts weakly with PSE-4 (data not shown). In addition, samples did not contain any proteinase inhibitor cocktail because we also observed that some inhibitors bind to the active site (data

not shown). Finally, no buffer was used because NMR data indicate that the phosphate buffer interacts weakly with TEM-1's active site (P.-Y. Savard and S. Gagné, personal communication, 2006), despite its ubiquitous use in many kinetics studies of β-lactamases. Therefore, samples were prepared to minimize any unwanted interaction that could bias our study because relaxation experiments are extremely sensitive.

As for the homologous TEM-1 (10), spectra were of very high quality despite PSE-4 molecular weight (Fig. S1). Backbone resonance assignments for PSE-4 (BMRB No. 6838) (17) allowed for the extraction of atom-specific data. Hence, no information could be extracted for residues Ser^{22}, Ser^{23}, Ser^{24}, Ser^{70}, and Ala^{237} for which assignments are unavailable; Ser^{22}, Ser^{23}, and Ser^{24}, probably because of fast solvent exchange; and Ser^{70} and Ala^{237}, certainly because of very broad and/or highly overlapped resonances. In addition, residues that overlapped severely were excluded from further analysis (see Table S2, Table S3, and Table S4). Hence, a total of 230 residues were characterized with data at the three magnetic fields ($N = 231$ at 50.6 MHz, 232 at 60.8 MHz, and 238 at 81.0 MHz).

^{15}N spin relaxation data

^{15}N spin relaxation data consisted of three sets of experiments: ^{15}N-R_1, ^{15}N-R_2, and $\{^1H\}^{15}N$ - NOE. Data at more than one magnetic field being required for overdetermination of model-free parameters, we acquired data at 11.7, 14.1, and 18.8 T (respectively, 50.6, 60.8, and 81.0 MHz nitrogen frequency). To confirm that the sample did not change during the experimental scheme, we recorded one set of NOE, three complete sets of R_1, and two complete sets of R_2 at 60.8 MHz before recording data at 50.6 and 81.0 MHz. After data acquisition at 50.6 and 81.0 MHz, we recorded two sets of NOE, one complete set of R_1, and three complete sets of R_2 again at 60.8 MHz. Moreover, it allowed us to verify that error on spin relaxation data was neither under- nor overestimated using Jackknife and Monte Carlo methods (data not shown). For example, the four different R_1 data sets recorded at 60.8 MHz gave rates that, within estimated errors, were reproducible for most residues. Mean relative errors for these data sets were as follows: 2.77%, 2.91%, 2.77%, and 3.28%. On the other hand, mean error for the combined data sets was 2.47%, reflecting the improvement obtained when using more data points. Data sets recorded at 50.6 and 81.0 MHz were not repeated as for 60.8 MHz (except for NOE at 50.6 MHz), but displayed errors of the same range. Finally, even though R_2 values obtained at 60.8 MHz were extracted from experiments with two different RF fields (5.2 and 6.0 kHz), this difference did not affect rates, which fell within respective errors (data not shown). ^{15}N spin relaxation data for PSE-4 have been deposited in the Biological Magnetic Resonance Data Bank (BMRB) (6838).

Statistics for the 2103 observables are available in Table S1. Mean errors for the recorded parameters vary between 2 and 4% before scaling (see Methods). Except for the five C-terminal residues, PSE-4 dynamics seems to be quite homogeneous, as is the case for TEM-1 (10). This points to a unique diffusion core for this enzyme.

Data sets consistency

To extract high quality information from multiple field experiments, it is important that data sets share a high degree of consistency. Inconsistencies can arise from several factors, including variations in sample viscosity (caused by changes in temperature, concentration, etc.) and water saturation during acquisition (which influences N-H moieties as a function of the exchange rate with the aqueous solvent). In this study, the field-independent function $J(0)$ (the spectral density at the zero frequency) (22) was used to assess data sets consistency.

Results from this consistency test demonstrate the good quality of the three data sets (Fig. S3). The 50.6 and 60.8 MHz data display especially high consistency, whereas 81.0 MHz consistency with 50.6 and 60.8 MHz data is good. The somehow wider distributions seen for data at 81.0 MHz were assessed further (see model-free analysis, below).

Model-free analysis

The model-free formalism (15,16,23,29) is the preferred approach for spin relaxation data analysis. Using this formalism, two main parameters, S^2 and τ, account, respectively, for the restriction of the motion for one vector (e.g., the N-H bond) and the effective upper limit for the timescale of this motion (normalized by S^2). Moreover, the R_{ex} parameter can account for slow motions on the μs-ms timescale contributing to the observed R_2. Several programs have been developed for the optimization of the model-free parameters. We used the open source program relax (23,24) with the protocol presented in Fig. S4.

A reanalysis of TEM-1's spin relaxation data (10) using the same approach as the one used here for PSE-4 has been performed recently and will be presented elsewhere. In this study, data were also reanalyzed using the same approach as in Savard and Gagné (10), but with ModelFree-4.20 (30,31) to avoid problems present in the preceding versions of the program (23). In the following discussion, results obtained for PSE-4 will be compared with those for TEM-1 in either publication, especially when differences arise.

Since the consistency test revealed some inconsistency in the 81.0 MHz data, an in-depth look at the data was done. We found out the R_2 data at 81.0 MHz were causing this inconsistency and did not use it for model-free analysis. Because the inconsistency was detected, it does not affect the quality of the extracted information. Details are available in the Supporting Material.

Description of global diffusion

The diffusion of PSE-4 is homogeneous. This is confirmed by the derivation of model-free parameters using a local

diffusion tensor for each N-H vector. Indeed, the mean local τ_m is 12.70 ± 0.87 ns (excluding the three C-terminal residues) with only a few dispersed outsiders, thus with no region in the three-dimensional structure showing differential diffusion (data not shown).

Table 1 shows a summary of the optimization results for the different diffusion tensors tested. The best model consists of an ellipsoid described by the isotropic component of diffusion $\mathbf{D}_{iso} = 13.141\ (\pm 0.024) \times 10^6\ s^{-1}$, the anisotropy of diffusion $\mathbf{D}_a = 3.75\ (\pm 0.19) \times 10^6\ s^{-1}$, the rhombicity $\mathbf{D}_r = 0.080\ (\pm 0.022)\ s^{-1}$, the global correlation time $\tau_m = 12.683\ (\pm 0.024)$ ns, and the diffusion constants for the three principal diffusion axes $\mathbf{D}_x = 11.59\ (\pm 0.10) \times 10^6\ s^{-1}$, $\mathbf{D}_y = 12.19\ (\pm 0.11) \times 10^6\ s^{-1}$, and $\mathbf{D}_z = 15.64\ (\pm 0.13) \times 10^6\ s^{-1}$. A representation of this diffusion tensor, and of the orientations of the N-H vectors used for its optimization, is available in Fig. S5. These parameters are close to the prolate description of TEM-1 presented in Savard and Gagné (10), where $\mathbf{D}_{||}/\mathbf{D}_{\perp}$ was equal to 1.23. Indeed, for PSE-4, $\mathbf{D}_{||}/\mathbf{D}_{\perp} = \mathbf{D}_z/((\mathbf{D}_x + \mathbf{D}_y)/2) = 1.32$. Anisotropy for PSE-4 extracted from the model-free analysis agrees with the shape from the crystal structure (14), the relative moments of inertia being 1.00, 0.89, and 0.59 as determined using the program pdbinertia (A. G. Palmer, Columbia University, New York, NY).

Finally, diffusion description from model-free analysis is close to that estimated from hydrodynamics calculations using HYDRONMR (32) (with parameter *a*, the effective radius of the atomic element, set to 2.6 Å, as in Hall and Fushman (33)). In fact, using this approach, $\mathbf{D}_a = 3.82 \times 10^6\ s^{-1}$, i.e., within 2% of model-free derived $\mathbf{D}_a$. Moreover, values of the diffusion constant for the three principal axes of the diffusion were within 4% of the model-free derived values, with $\mathbf{D}_{||}/\mathbf{D}_{\perp} = 1.30$. A similar analysis for TEM-1 is in agreement with PSE-4 having a higher anisotropy than TEM-1 and endorses model-free results for global tumbling.

Description of local motions

Fig. S6 shows the optimized residue-specific model-free parameters. Even though parameters are far more important than model listing, we can summarize PSE-4 local model-free models as follows: *m*0 (1), *m*1 (129), *m*2 (46), *m*3 (28), *m*4 (3), *m*5 (19), *m*6 (3), *m*7 (0), *m*8 (0), and *m*9 (1), for a total of 230 N-H vectors analyzed. As is seen here, most residues (77%) are fitted with simple models *m*1 and *m*2. Local model-free parameters for PSE-4 have been deposited in the BMRB.

TABLE 1 Summary of the diffusion tensor optimization

Diffusion model	AIC	τ_m (ns)	$D_{||}/D_{\perp}$	θ (°)	ϕ (°)	ψ (°)
Local τ_m	1442.1	—	—	—	—	—
Sphere	1492.2	12.39	1	—	—	—
Prolate spheroid	1391.3	12.67	1.33	147.5	50.1	—
Oblate spheroid	1475.6	12.45	0.92	38.9	27.2	—
Ellipsoid*	1385.1	12.68	1.32	166.2	146.8	131.6

We used 134 residues in regular secondary structures with relaxation data at three fields.

*Lowest AIC: selected description.

Order parameters

The mean order parameter (S^2) of PSE-4 backbone amides is 0.861 ± 0.087 (0.868 ± 0.051 excluding the three C-terminal flexible residues). Additionally, the mean S^2 for the secondary structure core (0.879 ± 0.035) is slightly higher and less dispersed than that for the loops and very short helices (0.834 ± 0.125; 0.852 ± 0.066 excluding the flexible C terminus). Clearly, PSE-4 is a highly ordered protein on the ps-ns timescale, displaying $S^2 > 0.85$ (the typical value for regular secondary structures, equivalent to motion on a cone of semiangle $\theta = 19°$ (15)) for 70% of its amides (Fig. 1 *A*). The most rigid amides are located around the active site and Ω loop, as was the case for TEM-1 (10). Only some solvent exposed loops are less rigid, with just five residues (Asn^{53}, Ser^{292}, Gln^{293}, Ser^{294}, and Arg^{295}) possessing an order parameter below 0.70, indicating the absence of high amplitude backbone motions in PSE-4, similar to previous observations for TEM-1. This high rigidity might be related to the low thermal stability of both TEM-1 and PSE-4, which precipitate in vitro at temperatures >41°C (data not shown).

When comparing TEM-1's model-free order parameters with those of PSE-4, TEM-1 appears slightly more rigid than PSE-4 (Fig. S8). Differences seem to be smaller for the Ω loop where order parameters agree more than for other loops, pointing to a conservation of order for this important part of the enzyme. This similarity of backbone dynamics on the ps-ns timescale might hide important differences for side-chain motions, as is the case for calmodulin (34). However, this is beyond the scope of this article.

Conformational exchange

Fig. 1 *B* shows residues for which a contribution to R_2 from μs-ms motions had to be accounted for. R_{ex} parameters depend on several factors (timescale of exchange, populations of either states, and chemical shift difference). Conformational exchange can be detected either for a moving N-H moiety or for a rigid vector with a moving neighbor modulating its chemical shift but can be invisible for certain combinations of timescales, populations, and chemical shift changes. R_{ex} parameters are scaled quadratically with the magnetic field and are presented in this study for an effective magnetic field of 60.8 MHz. Thus, R_{ex} values for TEM-1 (10) are rescaled from their originally associated field (50.6 MHz) for comparison purposes.

In PSE-4, 32 residues have a nonnull R_{ex} parameter. Of these, five are particularly important because of both their elevated R_{ex} parameter and localization on the protein three-dimensional structure. These are residues Thr^{128}, Leu^{221}, Arg^{234}, Ser^{235}, and Gly^{236}, which are located 4.5–12.5 Å from the active site. This is consistent with two nearby residues (Ser^{70} and Ala^{237}) not being observed,

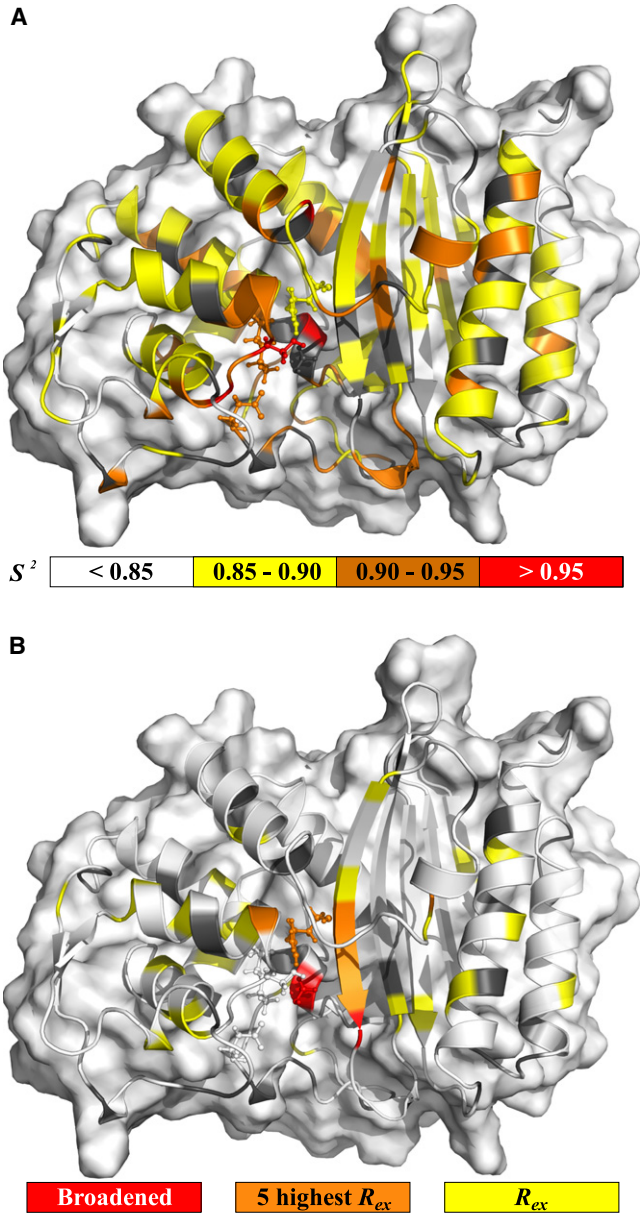

FIGURE 1 Motions extracted from model-free analysis. (*A*) Backbone amide ps-ns timescale generalized order parameter (S^2). (*B*) Residues fitted using a conformational exchange term (R_{ex}, model-free models *m*3, *m*4, *m*7, *m*8, or *m*9). In all insets, gray cartoon is used for residues without data (prolines, overlapped and unassigned) whereas, in the R_{ex} inset, white cartoon representation is used for absence of the parameter in the model fitted. Active site residues (Ser^{70}, Lys^{73}, Ser^{130}, Glu^{166}, and Arg^{234}) are shown in the stick representation. Missing residues in the crystal structure (Ser^{22}, Ser^{23}, Gln^{293}, Ser^{294}, and Arg^{295}) were added for visualization of their fitted parameters (refer to electronic figure for color representation).

probably because of their extreme broadening arising from important μs-ms motions. Since these motions are near the surface of the active site cavity, conformational exchange could arise because of a ligand moving in and out of the cavity. A potential candidate for this motion could be a structural water molecule moving slowly between residues Asn^{214}, Arg^{234}, and Ser^{235}, as seen in a 5-ns MD simulation of TEM-1 (35). This would point to a conservation of slow motions in the active site for both TEM-1 and PSE-4. The motion of this water molecule would also affect residues Ser^{70} and Ala^{237} (extremely broadened), both being on the path which the ligand would take to possibly access residues Asn^{214}, Arg^{234}, and Ser^{235}. The R_{ex} for Gly^{236} could be explained in the same way. The same is valid for TEM-1, where R_{ex} parameters arise near the active site and Ala^{237} could not be assigned.

Active-site residues

TEM-1's active site has been shown to be extremely ordered on the ps-ns timescale with several residues displaying order parameters >0.94 (10). This was consistent with active site residues displaying lower than average B-factors for TEM-1 in the presence of a sulfate ion in the active site (36). In PSE-4, the most rigid residues on the ps-ns timescale are also located in the active site, pointing to a meaningful conservation of this feature which could also be foreseen from backbone amide B-factors (14) (Fig. S7).

Ser^{70}: N-H correlation for Ser^{70} is not observed. In TEM-1, it is severely overlapped and broadened, thus unusable. This strongly supports the existence of motions on timescales slower than global tumbling (e.g., μs-ms) also affecting other residues in the vicinity that display broadened backbone (Ala237) or side-chain (Lys^{73}) resonances.

Lys^{73}: Lys^{73} is suspected of being involved in the first catalytic step (acylation), where its side-chain N_ζ group could activate Ser^{70} by accepting a proton from the side-chain hydroxyl group (2.8 Å away) (1). Lys^{73} was fitted to model *m*1 with one of the highest order parameters throughout PSE-4 (0.94 $\pm$ 0.01). This contrasts with the low intensity of its N-H cross-peak, which suggests that chemical exchange broadening may be present. Indeed, Lys^{73}'s C_α is the weakest of all lysine C_α (data not shown). Moreover, we were unable to see Lys^{73}'s side chain further than the C_β, thus preventing the titration of the side-chain N_ζ group. These, again, indicate important μs-ms motions nearby. These motions could be similar to those presumably affecting Ser^{70}, located <6 Å away (N-H to N-H). If rejecting model *m*1 because of these evidences of slow motions arising nearby, the second lowest size-corrected AIC score for Lys^{73} within PSE-4 is model *m*3 with an R_{ex} parameter of 0.7 $\pm$ 0.5 s^{-1}. Compared with the R_{ex} parameters for other residues, this R_{ex} would be the lowest and the one with the highest relative error. Hence, the possibility for Lys^{73} N-H to be fitted using an R_{ex} parameter is questionable, although strong signs of conformational exchange are present, especially for the side chain. The situation in TEM-1 was very similar, and Lys^{73} fitted model *m*1 with a S^2 of 0.95 $\pm$ 0.02. These data indicate Lys^{73}'s side chain could be affected by motions in the slow- or intermediate-exchange regime. Under certain conditions, R_{ex} does not scale quadratically with the magnetic field (37). This could explain the low R_{ex} with high error obtained for Lys^{73} when using model

$m3$, where the model-free fitting procedure scales the R_{ex} quadratically for multiple field data. Incorporating the parameter α from Millet et al. (37) in the fitting procedure could potentially alleviate this problem. Finally, if present, these motions could explain the extreme broadening of Lys^{73}'s side chain, as well as Ser^{70} and Ala^{237} amides. Such very slow motions will, in the future, be probed by relaxation dispersion experiments.

Tyr^{105}: Tyr^{105} displays a correlation time of 1008 ± 188 ps in conjunction with an S^2 of 0.80 ± 0.02 using the two-timescale model $m5$. In TEM-1, this residue was one of the most flexible (10) and the selected model did not incorporate this kind of two-timescale motion as in PSE-4. This could be of significant importance in regard to substrate recognition and specificity. The motion detected here could, however, be artefactual because model $m2$ also fits relatively well the experimental data: with a higher S^2 (0.85 ± 0.01), but with a correlation time of 26 ± 4 ps, similar to the case in TEM-1. On the other hand, model $m5$ could suit data almost as well in TEM-1, yielding a similar S^2 (0.79) but with a τ_s of ~500 ps.

In another work, Doucet et al. (38) discussed the importance of this residue for substrate specificity and proposed that steric restriction of the active site by residue Tyr^{105} side chain could allow the correct positioning and stabilization of substrates within the active site, thus facilitating catalysis. This gate-keeping function was further investigated and the side chain of Tyr^{105} was shown to adopt two conformations: one in which the side chain points toward Val^{216} (open state, rotamer t) and one in which the side chain points toward Glu^{104} (closed state, rotamer m, only visible in inhibitor-bound TEM-1) (39). This motion seen for TEM-1 could influence the dynamics of the backbone N-H moiety of Tyr^{105} in PSE-4 where rotamer t is present, with only minor electronic density toward the position of rotamer m. Using SHIFTS (Ver. 4.1.1) (40), chemical shifts for the two rotamers discussed in Doucet et al. (38) were predicted. Based on these results, only two residues would have their backbone ^{15}N chemical shift modified by such a transition between the two rotamers t and m. Of course, Tyr^{105} amide nitrogen has a different chemical shift in both rotamers, although the difference is very small (12 Hz at 60.8 MHz) and would not give rise to a significant R_{ex}. Ser^{106} would be more affected with a difference in ^{15}N chemical shift of 286 Hz at 60.8 MHz between the two rotamers. This would be expected to give rise to an R_{ex} term, although no such parameter was observed in the model-free minimization. A possible explanation for this situation is that the timescale for this conversion from rotamer t to rotamer m would be on the subnanosecond timescale as proposed by the selected model for Tyr^{105}. If so, it would not influence transverse relaxation of Ser^{106} and would only be probed by Tyr^{105} itself.

Ser^{130}: Residue Ser^{130} has been proposed to participate in the catalytic process (5) and was shown to be of clinical importance for enhanced resistance (41). In the crystal structure by Lim et al. (14), the hydroxyl group of Ser^{130} displays two alternative positions. Such alternative positions with a shared occupancy of 0.5 between two conformations are seen for eight other residues in the crystal structure (14). From model-free analysis, Ser^{130} fits model $m1$ (as other residues we could observe with atoms displaying shared occupancy of 0.5) with an S^2 of 0.95 ± 0.02. The movement of its side chain might not influence the amide transversal relaxation of Ser^{130}, but, depending on the timescale, could be the cause of such conformational exchange effects seen for nearby residues Ser^{70} (not observed, broadened), Thr^{128}, Arg^{234}, Ser^{235}, Gly^{236}, and Ala^{237} (not observed, broadened), all within 5 to 8 Å from the side chain of Ser^{130}. In TEM-1, no model-free parameter could be extracted (10). As for Lys^{73}, Ser^{130} order parameter in PSE-4 is very high. This is also the case for other residues of the conserved Ser^{130}-Asp^{131}-Asn^{132} (0.95 ± 0.02, 0.92 ± 0.01, and 0.97 ± 0.01, respectively) structural motif (known as the SDN loop).

Glu^{166}: Residue Glu^{166} is directly involved in catalysis, probably for both acylation and deacylation steps (1). As was the case for the two catalytic residues Lys^{73} and Ser^{130}, residue Glu^{166} fits model $m1$ with a fairly high order parameter (0.91 ± 0.02). In the reanalysis using ModelFree-4.20 for TEM-1, Glu^{166} fitted model $m1$ with $S^2 = 0.94 \pm 0.02$, in contrast with model $m4$ in the original work (10). Using relax, this residue was assigned model $m2$ with $S^2 = 0.93 \pm 0.02$ and $\tau_e = 47 \pm 24$ ps. This is not surprising, as the R_{ex} first detected was of low significance and, thus, $m4$ could simplify to $m1$ or $m2$. Rigidity for Glu^{166} thus seems similar in TEM-1, although a bit higher as for many other residues.

Arg^{234}: In carbenicillin-hydrolyzing β-lactamases such as PSE-4, residue 234 is an arginine. In other class-A β-lactamases, it is a lysine. Arg^{234} first fitted model $m2$ with an average S^2 of 0.88 ± 0.02. However, the value measured for R_2 at 50.6 MHz is most likely underestimated and erroneous, because of the partial overlap with residue Lys^{192}, a result of the poorer resolution at the lower field. Indeed, Arg^{234} has one of the highest R_2 values at both 60.8 and 81.0 MHz, whereas at 50.6 MHz the measured R_2 is much lower than for surrounding residues. Hence, when excluding R_2 at 50.6 MHz, the selected model becomes $m3$ with an unchanged order parameter of 0.88 and an R_{ex} parameter of $4.2 \pm 1.6\ s^{-1}$. This is much more logical for this residue, because the majority of surrounding residues display signs of conformational exchange. Moreover, for TEM-1, presence of R_{ex} was also found using either ModelFree-4.20 or relax, both with an R_{ex} of $1.9 \pm 0.4\ s^{-1}$ and a high S^2 of 0.94 ± 0.02. Thus, order on the ps-ns timescale would be higher in TEM-1, but the presence of slow μs-ms motions would be similar, again indicating the presence of conserved μs-ms motions near the active site.

Ω loop: A 19-residue loop is located below the active site of class-A β-lactamases (residues Arg^{161} to Asp^{179}). This loop is an Ω loop, a nonregular secondary structure found in many proteins (42). It was shown in two different studies to be flexible in TEM-1 using in silico approaches (35,43).

Indeed, in a 5-ns simulation (35), a flaplike motion of the Ω loop was present for TEM-1 in the absence of a ligand. The timescale was undefined in this study because this phenomenon was only seen once, the loop keeping its new position after the movement had happened. No such motion had been seen in the 1-ns simulation by Díaz et al. (44); these inconsistencies could either be a result of the short simulation length in the Díaz et al. (44) study or of simulation artifacts in the study of Roccatano et al. (35). Nevertheless, in TEM-1, using NMR, the Ω loop was shown to be very rigid on the ps-ns timescale, although displaying the presence of some μs-ms motions (10). This seems to unite short simulations results showing limited motions with longer simulations pointing to slow high-amplitude motions. Indeed, movements on the order of the μs-ms timescale are hardly defined using currently available MD simulations.

Our results for PSE-4 confirm this observation, although differently from what was seen in TEM-1 using NMR. In fact, only two residues within PSE-4 Ω loop display signs of conformational exchange (i.e., Arg^{161} and Arg^{178}). These residues are located at the extremities of the Ω loop, where it narrows (with N-H moieties separated by ~8 Å). Arg^{178} could represent the hinge of a movement similar to that stated above, which could allow Gly^{175} (Asn^{175} in TEM-1) to reach Arg^{65} to form the hydrogen bond discussed by Roccatano et al. (35) (Fig. 2). This would correspond to a movement of ~5 Å, Arg^{65} carbonyl being 7.1 Å from Gly^{175} amide nitrogen in the steady-state crystal structure. This motion would fill the cavity between the Ω loop and the protein core present in both TEM-1 and PSE-4 (Fig. 2 *D*). With this cavity closed, the structure would be better packed, possibly transiently stabilizing Glu^{166} in a catalytically relevant position. The absence of R_{ex} for residues Asp^{176} and Leu^{177} does not counterindicate this possibility, as the N-H moiety of Leu^{177} would point toward the solvent in both conformations and hydrogen bonding of Asp^{176} N-H group with the carbonyl of residue Lys^{173} would also be present in both conformations. Unfortunately, because of overlapped resonances, no spin relaxation data are available for residues Lys^{173} and Leu^{174}, which could sense this movement because they are closer to the protein core. However, these residues both display normal amplitude N, H^N, C_α, and C_β resonances, which could contradict their involvement into conformational exchange. Hence, current observations support the slow motion of the Ω loop proposed by Roccatano et al. (35). Because of the implications of movements of the Ω loop in terms of catalysis, it will be very important to get more insights into this part of the enzyme. In fact, if a movement such as the one discussed above exists, it would allow Glu^{166} to stay close to Ser^{70} and potentially act during the acylation step (35).

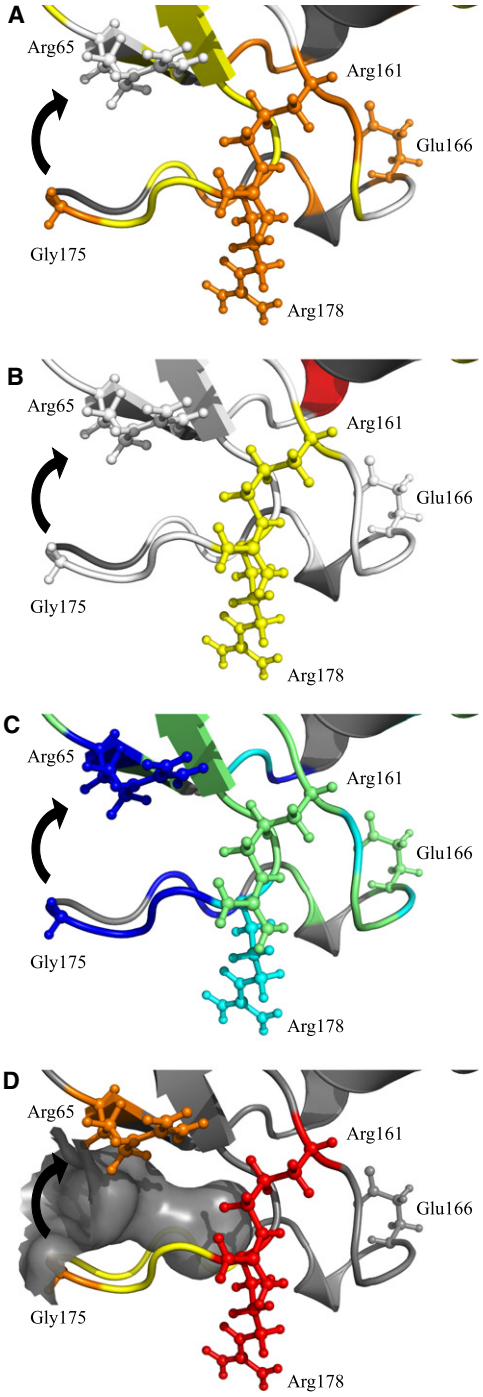

FIGURE 2 Cavity-filling motion for residues Glu^{171}-Leu^{177} of the Ω loop. (*A*) Order parameters (S^2 colored as in Fig. 1 *A*). (*B*) Conformational exchange (R_{ex} colored as in Fig. 1 *B*). (*C*) Apparent free energies of exchange (ΔG_{HX}, colored as in Fig. 3). (*D*) The cavity between the Ω loop and the protein core that the motion of residues Glu^{171}-Leu^{177} (*yellow*) would fill is shown in gray surface. Residues from the hinge (Arg^{161} and Arg^{178}) are colored red and shown in the stick representation as well as residues Arg^{65} and Gly^{175} (*orange*), which would form a hydrogen bond once the motion (*black arrow*) is completed. Catalytic Glu^{166} is also shown in the stick representation. A stereo version is available in the Supporting Material.

Limits in the analytical approach

Many factors limit interpretation of results extracted using the model-free approach (23,24). Here, we will concentrate

on three specific limitations: variations of the CSA and r_{N-H} for different N-H moieties, and lack of well-defined N-H vector orientations in crystal structures. In this study, the CSA was held fixed with a value of −172 ppm. This allowed comparison with dynamics data for TEM-1 (10). As for the CSA, r_{N-H} was held fixed with a value of 1.02 Å, which allowed comparison with dynamics data for TEM-1 (10). Further discussion on CSA and r_{N-H} is available in the Supporting Material. Crystal structure 1G68 (14) has a 1.95 Å resolution, which does not allow the visualization of protons. Hence, derived N-H vector orientations may be erroneous from their actual average position, potentially having an effect on the model-free models selected because goodness of fit depends on N-H vector orientation compared to the diffusion tensor orientation. Moreover, for residues potentially involved in crystal contacts, orientations might be slightly off, which could also bias model-free analysis. This situation could be assessed by allowing variation of N-H bond orientations during model-free minimization. However, we chose not to introduce such variable into our analysis.

Amide exchange

Steady-state amide exchange experiments allow the study of higher energy states, difficult to detect with techniques reporting on ensembles. They can probe the presence of partially unfolded states, intermediates of which could be of importance for catalysis. Two limit cases for amide exchange exists: EX1 and EX2 (45). In the EX2 regime, insights into the thermodynamics of the opening reaction for the structure protecting the N-H group from exchange (transient unfolding processes) can be obtained. The equilibrium constant of exchanging sites $K_{op} = 1/SF = k_{open}/k_{close}$, where SF is the protection factor, and k_{open} and k_{close} the opening and closing rates, respectively, is calculated from $K_{op} = k_{ex}/k_c$, where k_{ex} is the exchange rate, and k_c is the expected unprotected exchange rate (intrinsic rate) (46,47). Moreover, the apparent stabilization free energy of the protecting structure is obtained from $\Delta G_{HX} = -RT \ln K_{op}$.

In the EX2 regime, exchange rates are pH-dependent, whereas in the EX1 limit, they are not affected by pH. Exchange was faster at pH 7.85 for all residues for which data were available, hence confirming the EX2 regime at pH 6.65 (see Table S4 and Fig. S9). A change of pH from 6.65 to 7.85 would theoretically cause effective rates to increase by a factor of 16. The mean increase of k_{ex}, in our case, was of 11 ± 7 (not including amides exchanging too fast to be observed at pH 7.85). This lower value could be a result of some amides entering the EX1 regime at a pH slightly below 7.85. Of the 226 residues with available data at pH 6.65, 101 exchanged very rapidly and were already unobservable in the first time point (i.e., after only 32 min, with $k_{ex} > 1 \times 10^{-3}$ s^{-1}). Therefore, 125 residues had a measurable exchange rate ranging from 2×10^{-3} s^{-1} to 3×10^{-8} s^{-1}. ΔG_{HX}, as well as K_{op} and SF, were calculated using an Excel spreadsheet from S. W. Englander (University of Pennsylvania, Philadelphia, PA) and are displayed in Table S4. Moreover, ΔG_{HX} values are shown in Fig. 3. These data have been deposited in the BMRB (6838).

Globally, free energies of opening are ~6–11 kcal mol^{-1} for most residues within secondary structures, and are slightly higher in the α/β domain where many residues have $\Delta G_{HX} > 8$ kcal mol^{-1}. Hence, this domain is more stable than the all α-domain. This is contrary to what was proposed for TEM-1 (10), that the α-domain might be the most stable. This hypothesis was speculative, as no amide exchange rate had been extracted, nor verification of EX2 regime done. For TEM-1, the slowest exchanging amides were those from the all α-domain and the authors concluded that this domain is more stable than the α/β domain because of the presence of the disulfide bond between Cys^{77} and Cys^{123}, as proposed by Vanhove et al. (48). Here, we postulate the contrary for PSE-4 based on EX2 exchange data. In PSE-4, though the disulfide bond between Cys^{77} and Cys^{123} stabilizes the local structure (surrounding residues with ΔG_{HX} between 4 and 8 kcal mol^{-1}), the protection from the solvent in the α-domain is globally lower than in the α/β domain. One might argue that the disulfide bond in the PSE-4 sample is not formed. However, this is ruled out by C_β chemical shifts (49) for Cys^{77} (41.6 ppm) and Cys^{123} (42.0 ppm) (17), which show that both Cys are oxidized. The most stable domain in PSE-4 is the α/β domain, whereas

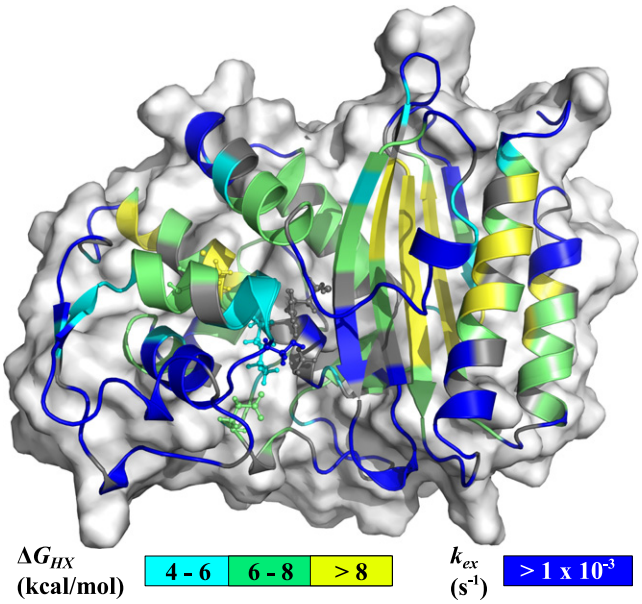

FIGURE 3 Apparent stabilization free energies of the protecting structures (ΔG_{HX}). The value k_{ex} is shown for residues for which exchange was too fast for being quantified ($k_{ex} > 1 \times 10^{-3}$ s^{-1}). Important active site residues (Ser^{70}, Lys^{73}, Ser^{130}, Glu^{166}, and Arg^{234}) and the disulfide bond (between Cys^{77} and Cys^{123}, connecting two helices of the α-domain) are shown in the stick representation. Missing residues in the crystal structure (Ser^{22}, Ser^{23}, Gln^{293}, Ser^{294}, and Arg^{295}) were added for visualization of their parameters.

it could be the α-domain in TEM-1. Indeed, theoretical free energy of folding calculated using VADAR (50) shows that the all α-domain in TEM-1 would be more stable than in PSE-4, whereas the inverse is predicted for the α/β domain (data not shown). These could indicate some thermodynamics differences between the two domains of these homologs. However, to confirm this hypothesis, analysis of data in the EX2 regime is required for TEM-1.

As expected, the first protons to exchange with the solvent were those within loops as well as most key residues from the active site (Fig. 3). Moreover, all glutamine and asparagine side chains were exchanged rapidly. These N-H moieties being all located at or near the protein surface, their exchange is too fast for steady-state exchange experiments and would require approaches such as pulse labeling (45). It is interesting to note that all residues from the Ile^{97} to Gln^{115} region exchange fast, as well as residues Asn^{132} to Ile^{137} from the adjacent α-helix. This region of PSE-4 could have a nonnegligible population existing as a partially unfolded state (probably with $\Delta G_{HX} < 4$ kcal mol^{-1}, k_{ex} values all being $>1 \times 10^{-3}$ s^{-1}, despite 17 amides out of 24 having null ASA, as calculated using VADAR (50)). Indeed, ΔG_{HX} below 4 kcal mol^{-1} would correspond to populations of partially unfolded states for >0.1%. Thus, the subdomain formed by residues Ile^{97} to Gln^{115} and Asn^{132} to Ile^{137} could be the driving force for the lower stability of the close by α-domain. Hence, local unfolding could arise near the active site, including residue Tyr^{105}, for which motions were discussed above. These local unfolding events, from both their population and their possible timescale and location could have a profound impact on PSE-4 catalysis and might be the cause of some of the observed R_{ex}.

The fact that the amide of Glu^{166} and a few other amides from the Ω loop are protected from exchange with ΔG_{HX} between 6 and 8 kcal mol^{-1} points toward some motional restriction of this long loop, preventing the disruption of the network of hydrogen bonds and the exposure of amide moieties to solvent. This argues against μs-ms motions proposed for TEM-1 in Savard and Gagné (10), where residues Arg^{164}, $Glu^{166,}$ and Leu^{169} possessed a R_{ex} parameter, these three residues displaying ΔG_{HX} of 7.3, 7.6, and 6.1 kcal mol^{-1}, respectively, within PSE-4. However, this is in agreement with the motion proposed by Roccatano et al. (35) and discussed in the model-free analysis, above, where residues Glu^{171}-Leu^{177} (with $k_{ex} > 1 \times 10^{-3}$ s^{-1}) could move toward the protein core without affecting residues Arg^{161}-Glu^{170} (with mean ΔG_{HX} ~6.7 kcal mol^{-1}), as shown in Fig. 2. Indeed, this motion could transiently position the Ω loop so Glu^{166} is in the vicinity of Ser^{70} (35). Moreover, the loop could be protected against complete hydration. In fact, as stated before, at the location where residues Glu^{171}-Leu^{177} are proposed to translate by this motion, a cavity is present (Fig. 2 *D*). This available space would be filled in the closed state. The same cavity being also present in TEM-1, the conservation of this motion among class A β-lactamases is plausible, in agreement with observations from Roccatano et al. (35), as well as with recent simulations of both TEM-1 and PSE-4 which show motions of a different nature for the Ω loop, also consistent with our experimental data (O. Fisette and S. Gagné, personal communication, 2008). Finally, the fact that this motion was only seen once during the 5-ns simulation is consistent with a much slower effective timescale, as suggested by R_{ex} parameters extracted from model-free analysis.

Finally, during model-free analysis, Ser^{235} and Gly^{236}, which both exchange with rates faster than 1×10^{-3} s^{-1}, were fitted with high R_{ex} parameters (7.5 and 4.5 s^{-1}, respectively). These data, in addition to null ASA for these amides, support the presence of μs-ms motions near the active site, potentially severely broadening amide cross-peaks of residues Ser^{70} and Ala^{237}, as discussed before. Once again, these motions might be important for catalysis since k_{cat} for hydrolysis of β-lactams by β-lactamases is ~1 ms^{-1}.

CONCLUSIONS

This work is the first NMR characterization, to our knowledge, of the dynamics of a class A carbenicillin hydrolyzing β-lactamase. It follows the study of Savard and Gagné (10), which explored the dynamics of another class A β-lactamase, TEM-1.

Linking results from the different techniques used here to PSE-4 catalytic activity is not straightforward (51). The global picture of PSE-4 depicted in this report shows a very rigid protein on several timescales. Indeed, ps-ns timescale order parameters are elevated, almost as much as in the case of the homologous TEM-1. Moreover, overall stability is also quite elevated, with apparent free energies of opening (from amide exchange experiments) reaching 11 kcal mol^{-1} for several residues in the β-sheet of the α/β domain. These results contrast with the low thermal stability of both TEM-1 and PSE-4 and with the presence of slow μs-ms motions.

Rigidity on the ps-ns timescale could be a characteristic of all class A β-lactamases. As stated before, the catalytic efficiency of some of the class A β-lactamases is diffusion controlled (3). This high efficiency supplemented by a high plasticity toward different types of β-lactams contrasts with the restricted motions in the catalytic site, at least on the ps-ns timescale. Longer timescales might be populated by important conserved motions as shown for many active site residues displaying conformational exchange terms (R_{ex}) reporting on the μs-ms timescale, the timescale of enzyme catalysis (e.g., PSE-4's k_{cat} against ampicillin and carbenicillin is ~1.2 ms^{-1} (52)). Moreover, the absence of detectable high amplitude motions on the faster timescales might show that the active site of class A β-lactamases adapts its shape on substrate approach, thus pointing to motions present during some steps of the catalytic process. To further understand this feature, it will be interesting to get insights into those longer timescales and to study dynamics of TEM-1 and

PSE-4 mutants. Moreover, it will be critical to obtain data regarding dynamics during catalysis (see below).

We are aware that backbone dynamics can be decoupled from side-chain motions (34). The apparent lack of motions seen for backbone N-H moieties on the ps-ns timescale could be coupled to important side-chain motions on the same timescale. In addition, the apparent dynamics similarity between TEM-1 and PSE-4 might also prove limited to backbone amides with side chains potentially displaying different motional patterns. Hence, a side-chain dynamics study might prove very insightful. Moreover, we are mindful about the lack of data for a bound form of PSE-4 either with a β-lactam or an inhibitor. However, as highlighted by Savard and Gagné (10), this proves to be very difficult, considering the high catalytic efficiency of these enzymes. Finally, we are aware that conformational exchange indications showed here are qualitative and extracted from the transversal relaxation rates variations over a restricted range of magnetic field strengths. Hence, the μs-ms timescale will be an interesting target for further studies to better quantify the slow motions detected here, especially for what concerns motions around the Ω loop and active site cavity. This will be quite interesting, as this timescale is where the cleavage of the β-lactam ring occurs. Thus, the recording of relaxation dispersion data will certainly shed light onto the conformational exchange processes suspected to arise near the active site. Here, some residues (e.g., Lys^{73}), although rigid on the ps-ns timescale, display broadened resonances, in addition to some resonances even being invisible, as a result of peak broadening (e.g., Ser^{70}).

Finally, the detailed backbone dynamics data gathered for PSE-4 will join those from TEM-1 in enabling in-depth MD simulations. A comparative study of PSE-4 backbone dynamics characterized by MD and NMR is currently underway. This will permit better in silico studies of the dynamics of class A wild-type and mutant β-lactamases in the presence of substrate, experiments which are impossible using NMR because the turnover rate of relevant β-lactams is tremendously fast with respect to NMR experiments being quite long.

SUPPORTING MATERIAL

PSE-4 raw relaxation and amide exchange data as well as model-free analysis results are part of the supporting material. Four tables and 10 figures are available at http://www.biophysj.org/biophysj/supplemental/S0006-3495(09)00699-7.

We thank Edward d'Auvergne for many reasons, among which are interesting discussions on NMR theory (and for relax), and we thank Pierre-Yves Savard, Olivier Fisette, Richard Daigle, Nicolas Doucet, Tara Sprules, Roger C. Levesque, and Pierre Lavigne for stimulating discussions.

This work was supported by operating grants from Fonds de la Recherche en Santé du Québec and the Natural Sciences and Engineering Research Council of Canada, infrastructure grants from Canada Foundation for Innovation (both Innovation and New Opportunity), and studentships to S. Morin from the Natural Sciences and Engineering Research Council of Canada, Fonds de la Recherche en Santé du Québec, and Fondation J.-Arthur Vincent.

REFERENCES

1. Fisher, J. F., S. O. Meroueh, and S. Mobashery. 2005. Bacterial resistance to β-lactam antibiotics: compelling opportunism, compelling opportunity. *Chem. Rev.* 105:395–424.
2. Matagne, A., J. Lamotte-Brasseur, and J. M. Frère. 1998. Catalytic properties of class A β-lactamases: efficiency and diversity. *Biochem. J.* 330:581–598.
3. Christensen, H., M. T. Martin, and S. G. Waley. 1990. β-lactamases as fully efficient enzymes. Determination of all the rate constants in the acyl-enzyme mechanism. *Biochem. J.* 266:853–861.
4. Hedstrom, L. 2002. Serine protease mechanism and specificity. *Chem. Rev.* 102:4501–4524.
5. Oefner, C., A. D'Arcy, J. J. Daly, K. Gubernator, R. L. Charnas, et al. 1990. Refined crystal structure of β-lactamase from *Citrobacter freundii* indicates a mechanism for β-lactam hydrolysis. *Nature.* 343:284–288.
6. Meroueh, S. O., J. F. Fisher, H. B. Schlegel, and S. Mobashery. 2005. Ab initio QM/MM study of class A β-lactamase acylation: dual participation of Glu^{166} and Lys^{73} in a concerted base promotion of Ser^{70}. *J. Am. Chem. Soc.* 127:15397–15407.
7. Allerhand, A., D. Doddrell, V. Glushko, D. W. Cochran, E. Wenkert, et al. 1971. Conformation and segmental motion of native and denatured ribonuclease A in solution. Application of natural-abundance carbon-13 partially relaxed Fourier transform nuclear magnetic resonance. *J. Am. Chem. Soc.* 93:544–546.
8. Wand, A. J. 2001. Dynamic activation of protein function: a view emerging from NMR spectroscopy. *Nat. Struct. Biol.* 8:926–931.
9. Yon, J. M., D. Perahia, and C. Ghélis. 1998. Conformational dynamics and enzyme activity. *Biochimie.* 80:33–42.
10. Savard, P.-Y., and S. M. Gagné. 2006. Backbone dynamics of TEM-1 determined by NMR: evidence for a highly ordered protein. *Biochemistry.* 45:11414–11424.
11. Doucet, N., P.-Y. Savard, J. N. Pelletier, and S. M. Gagné. 2007. NMR investigation of Tyr^{105} mutants in TEM-1 β-lactamase: dynamics are correlated with function. *J. Biol. Chem.* 282:21448–21459.
12. Newsom, S. W. 1969. Carbenicillin-resistant *Pseudomonas*. *Lancet.* 2:1141.
13. Reid, A. J., I. N. Simpson, P. B. Harper, and S. G. Amyes. 1988. The differential expression of genes for the PSE-4 β-lactamase in *Pseudomonas aeruginosa* and the *Enterobacteriaceae*. *J. Antimicrob. Chemother.* 21:525–533.
14. Lim, D., F. Sanschagrin, L. Passmore, L. D. Castro, R. C. Levesque, et al. 2001. Insights into the molecular basis for the carbenicillinase activity of PSE-4 β-lactamase from crystallographic and kinetic studies. *Biochemistry.* 40:395–402.
15. Lipari, G., and A. Szabo. 1982. Model-free approach to the interpretation of nuclear magnetic resonance relaxation in macromolecules. 1. Theory and range of validity. *J. Am. Chem. Soc.* 104:4546–4559.
16. Lipari, G., and A. Szabo. 1982. Model-free approach to the interpretation of nuclear magnetic resonance relaxation in macromolecules. 2. Analysis of experimental results. *J. Am. Chem. Soc.* 104:4559–4570.
17. Morin, S., R. Levesque, and S. M. Gagné. 2006. ^{1}H, ^{13}C, and ^{15}N backbone resonance assignments for PSE-4, a 29.5 kDa class A β-lactamase from *Pseudomonas aeruginosa*. *J. Biomol. NMR.* 36 (Suppl 1):11.
18. Kay, L. E., P. Keifer, and T. Saarinen. 1992. Pure absorption gradient enhanced heteronuclear single quantum correlation spectroscopy with improved sensitivity. *J. Am. Chem. Soc.* 114:10663–10665.
19. Farrow, N. A., R. Muhandiram, A. U. Singer, S. M. Pascal, C. M. Kay, et al. 1994. Backbone dynamics of a free and phosphopeptide-complexed Src homology 2 domain studied by ^{15}N NMR relaxation. *Biochemistry.* 33:5984–6003.
20. Tjandra, N., P. Wingfield, S. Stahl, and A. Bax. 1996. Anisotropic rotational diffusion of perdeuterated HIV protease from ^{15}N NMR relaxation measurements at two magnetic fields. *J. Biomol. NMR.* 8:273–284.

21. Delaglio, F., S. Grzesiek, G. W. Vuister, G. Zhu, J. Pfeifer, et al. 1995. NMRPipe: a multidimensional spectral processing system based on UNIX pipes. *J. Biomol. NMR.* 6:277–293.
22. Farrow, N., O. Zhang, A. Szabo, D. Torchia, and L. E. Kay. 1995. Spectral density function mapping using ^{15}N relaxation data exclusively. *J. Biomol. NMR.* 6:153–162.
23. d'Auvergne, E. J., and P. R. Gooley. 2008. Optimization of NMR dynamic models. I. Minimization algorithms and their performance within the model-free and Brownian rotational diffusion spaces. *J. Biomol. NMR.* 40:107–119.
24. d'Auvergne, E. J., and P. R. Gooley. 2008. Optimization of NMR dynamic models. II. A new methodology for the dual optimization of the model-free parameters and the Brownian rotational diffusion tensor. *J. Biomol. NMR.* 40:121–133.
25. Kabsch, W., and C. Sander. 1983. Dictionary of protein secondary structure: pattern recognition of hydrogen-bonded and geometrical features. *Biopolymers.* 22:2577–2637.
26. Akaike, H.1973. Information theory and an extension of the maximum likelihood principle. *In* Proceedings of the 2nd International Symposium on Information Theory, Budapest, Hungary. B.N. Petrov and F. Csaki, editors.
27. Hurvich, C., and C.-L. Tsai. 1989. Regression and time series model selection in small samples. *Biometrika.* 76:297–307.
28. Ambler, R. P., A. F. Coulson, J. M. Frère, J. M. Ghuysen, B. Joris, et al. 1991. A standard numbering scheme for the class A β-lactamases. *Biochem. J.* 276:269–270.
29. Clore, G. M., A. Szabo, A. Bax, L. E. Kay, P. C. Driscoll, et al. 1990. Deviations from the simple two-parameter model-free approach to the interpretation of Nitrogen-15 nuclear magnetic-relaxation of proteins. *J. Am. Chem. Soc.* 112:4989–4991.
30. Palmer, A., M. Rance, and P. Wright. 1991. Intramolecular motions of a zinc finger DNA-binding domain from Xfin characterized by proton-detected natural abundance ^{13}C heteronuclear NMR spectroscopy. *J. Am. Chem. Soc.* 113:4371–4380.
31. Mandel, A. M., M. Akke, and A. G. Palmer. 1995. Backbone dynamics of *Escherichia coli* ribonuclease HI: correlations with structure and function in an active enzyme. *J. Mol. Biol.* 246:144–163.
32. García de la Torre, J., M. L. Huertas, and B. Carrasco. 2000. HYDRONMR: prediction of NMR relaxation of globular proteins from atomic-level structures and hydrodynamic calculations. *J. Magn. Reson.* 147:138–146.
33. Hall, J. B., and D. Fushman. 2003. Characterization of the overall and local dynamics of a protein with intermediate rotational anisotropy: differentiating between conformational exchange and anisotropic diffusion in the B3 domain of protein G. *J. Biomol. NMR.* 27:261–275.
34. Lee, A. L., S. A. Kinnear, and A. J. Wand. 2000. Redistribution and loss of side chain entropy upon formation of a calmodulin-peptide complex. *Nat. Struct. Biol.* 7:72–77.
35. Roccatano, D., G. Sbardella, M. Aschi, G. Amicosante, C. Bossa, et al. 2005. Dynamical aspects of TEM-1 β-lactamase probed by molecular dynamics. *J. Comput. Aided Mol. Des.* 19:329–340.
36. Jelsch, C., L. Mourey, J. M. Masson, and J. P. Samama. 1993. Crystal structure of *Escherichia coli* TEM1 β-lactamase at 1.8 Å resolution. *Proteins.* 16:364–383.
37. Millet, O., J. Loria, C. Kroenke, M. Pons, and A. Palmer. 2000. The static magnetic field dependence of chemical exchange linebroadening defines the NMR chemical shift time scale. *J. Am. Chem. Soc.* 122:2867–2877.
38. Doucet, N., P.-Y. De Wals, and J. N. Pelletier. 2004. Site-saturation mutagenesis of Tyr-105 reveals its importance in substrate stabilization and discrimination in TEM-1 β-lactamase. *J. Biol. Chem.* 279:46295–46303.
39. Doucet, N., and J. N. Pelletier. 2007. Simulated annealing exploration of an active-site tyrosine in TEM-1 β-lactamase suggests the existence of alternate conformations. *Proteins.* 69:340–348.
40. Xu, X. P., and D. A. Case. 2001. Automated prediction of ^{15}N, $^{13}C_{\alpha}$, $^{13}C_{\beta}$ and $^{13}C'$ chemical shifts in proteins using a density functional database. *J. Biomol. NMR.* 21:321–333.
41. Lahey Clinic. TEM extended-spectrum and inhibitor resistant β-lactamases. www.lahey.org/Studies/temtable.asp.
42. Fetrow, J. S. 1995. Omega loops: nonregular secondary structures significant in protein function and stability. *FASEB J.* 9:708–717.
43. Vijayakumar, S., G. Ravishanker, R. F. Pratt, and D. L. Beveridge. 1995. Molecular dynamics simulation of a class A β-lactamase: structural and mechanistic implications. *J. Am. Chem. Soc.* 117:1722–1730.
44. Díaz, N., T. L. Sordo, K. M. Merz, Jr., and D. Suárez. 2003. Insights into the acylation mechanism of class A β-lactamases from molecular dynamics simulations of the TEM-1 enzyme complexed with benzylpenicillin. *J. Am. Chem. Soc.* 125:672–684.
45. Krishna, M. M. G., L. Hoang, Y. Lin, and S. W. Englander. 2004. Hydrogen exchange methods to study protein folding. *Methods.* 34:51–64.
46. Bai, Y., J. S. Milne, L. Mayne, and S. W. Englander. 1993. Primary structure effects on peptide group hydrogen exchange. *Proteins.* 17:75–86.
47. Connelly, G. P., Y. Bai, M. F. Jeng, and S. W. Englander. 1993. Isotope effects in peptide group hydrogen exchange. *Proteins.* 17:87–92.
48. Vanhove, M., G. Guillaume, P. Ledent, J. H. Richards, R. H. Pain, et al. 1997. Kinetic and thermodynamic consequences of the removal of the Cys-77-Cys-123 disulphide bond for the folding of TEM-1 β-lactamase. *Biochem. J.* 321:413–417.
49. Sharma, D., and K. Rajarathnam. 2000. ^{13}C NMR chemical shifts can predict disulfide bond formation. *J. Biomol. NMR.* 18:165–171.
50. Willard, L., A. Ranjan, H. Zhang, H. Monzavi, R. F. Boyko, et al. 2003. VADAR: a web server for quantitative evaluation of protein structure quality. *Nucleic Acids Res.* 31:3316–3319.
51. Jarymowycz, V. A., and M. J. Stone. 2006. Fast time scale dynamics of protein backbones: NMR relaxation methods, applications, and functional consequences. *Chem. Rev.* 106:1624–1671.
52. Sabbagh, Y., E. Thériault, F. Sanschagrin, N. Voyer, T. Palzkill, et al. 1998. Characterization of a PSE-4 mutant with different properties in relation to penicillanic acid sulfones: importance of residues 216 to 218 in class A β-lactamases. *Antimicrob. Agents Chemother.* 42:2319–2325.